

**On the Mechanics and Thermodynamics of a
Low-Level Wave on the Easterlies**

by
Russell Elsberry

A report of Research Performed under a Grant by Environmental Science Services
Administration to Colorado State University
Grant No. WBG-61

Technical Paper No. 101
Department of Atmospheric Science
Colorado State University
Fort Collins, Colorado

May 1966

**Colorado
State
University**

**Department of
Atmospheric Science**

Paper No. 101

On the Mechanics and Thermodynamics of a
Low-Level Wave on the Easterlies

by

Russell Elsberry
Colorado State University

A Report on Research Performed Under a
Grant by Environmental Science Services
Administration to Colorado State University

Grant No. WBG-61

Fort Collins, Colorado

May 1966

Atmospheric Science Paper No. 101

ABSTRACT

In order to gain background on the constraints on hurricane development from waves in the easterlies, a warm-core wave observed in the Caribbean was studied. Data were composited with respect to the wave axis for three days assuming nearly a steady state. The synoptic scale structure and energetics are discussed. The kinetic energy balance indicates an excess of production over the computed dissipation. A heat balance of the system likewise shows an excess heat source. Models of the meso-scale cloud structure required to balance the heat budget under constraint of kinetic energy balance are proposed.

Introduction

In recent years interest in waves in the easterlies as an initial step in the development of hurricanes has been renewed. The approaches to the hurricane development problem have been varied, including numerous attempts at numerical simulation with high speed computers. A common starting point of the numerical investigations is a pre-existing disturbance. A common result of most of these investigations has been development of a hurricane-like circulation--it appears relatively easy to develop a hurricane with a computer, but nature finds it more difficult. Here we wish to examine the problem of constraint on development by means of a synoptic investigation of a wave in the easterlies.

During September, 1963, Dr. H. Riehl observed from San Juan the passage of such a wave. This particular wave possessed clouds to 20,000 feet with only a few cumulonimbi. Although total rainfall was light, rather strong showers were observed. An examination of the synoptic maps showed a well-defined wave at the surface which decreased in intensity with height into nearly zonal flow above 700-600 mb. Thus the wave appeared to be of the warm-core type, the occurrence of which was thought to be rather infrequent, but has since been noted to occur in other years. The purpose of this report is to give a description of such a warm-core wave in the easterlies, and to investigate the constraints which prevented development of a disturbance that already possessed the warm-core structure observed in pre-hurricane depressions.

DATA COVERAGE AND HANDLING

Whereas the Caribbean network (Figure 1) has perhaps the best data coverage of any area in the tropics, there remain gaps in the network which have generally prevented detailed synoptic analysis of waves in the easterlies. The present wave appeared to move in nearly steady state from 1200 GMT, September 12, when it entered the data network, until it moved over Cuba on the 15th. Figure 1 shows the axis of the wave as it was reconstructed from the surface weather maps. On any particular day the data coverage was not sufficient to allow detailed analysis. Consequently use was made of the nearly steady state conditions to composite the data with respect to the wave.

An example of the resulting coverage is shown in Figure 2, which shows the 850 mb winds. Composites were made at 1000, 925, 850, 775, 700, and 600 mb of the reported winds, temperatures, and specific humidities. The coverage on the temperature and moisture composites was

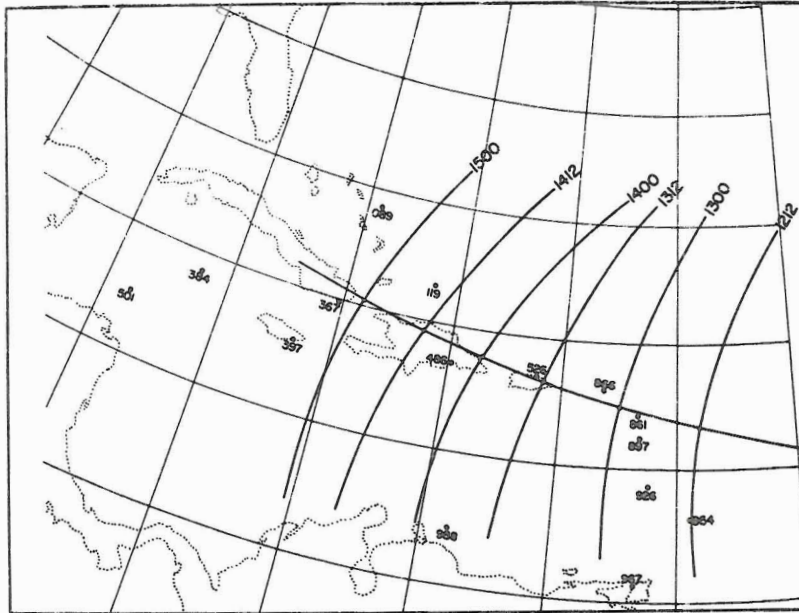


Figure 1. Map of the caribbean showing the stations which were used in the study. Heavy lines show positions of the axis of the wave in the easterlies at successive map times (1500 indicates 00 GMT on September 15)

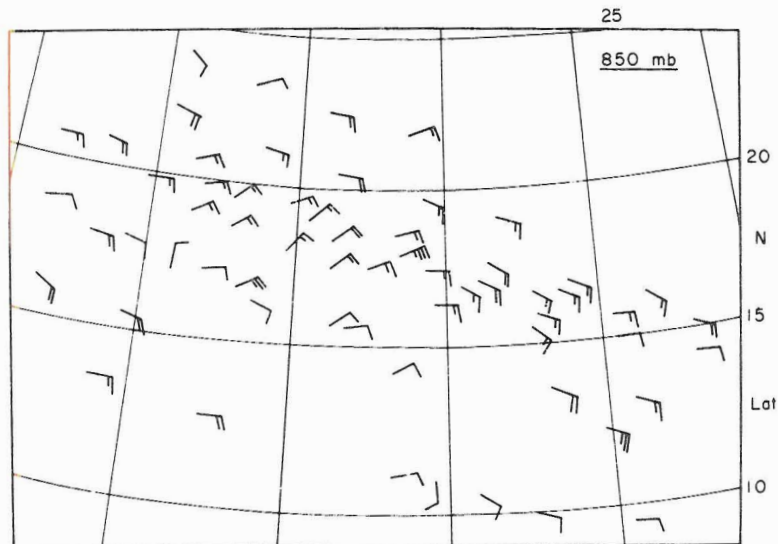


Figure 2. Example of data coverage showing the composite with respect to the wave axis of the reported 850 mb winds. Latitude and longitude lines for the middle time period are superimposed for orientation only.

not as good as in Figure 2, in which pilot balloon reports were used with the rawinsonde ascents.

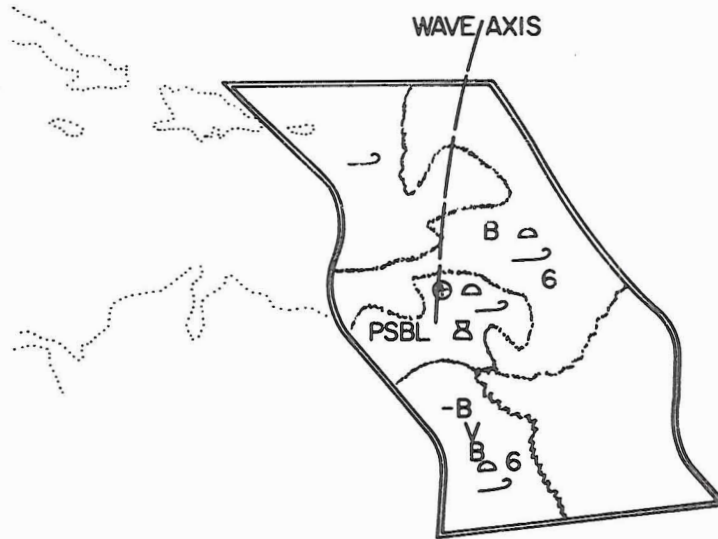
Satellite photographs from the Tiros series have been used in studies of waves in the easterlies (e.g. Merritt, 1964; Fett, 1965). Several passes of Tiros VI and VII produced good coverage of the wave axis on September 12 and 14. On September 12 (Figure 3a) the clouds were quite dense east of the wave typical of the "classical" type. On September 14 (Figure 3b) the clouds appeared to shift in response to the approach of a middle latitude trough.

Time sections, long a basic tool of the tropical meteorologist (Riehl, 1945), were used to verify the positions of the wave axis shown in Figure 1. The time section for St. Maarten (Figure 4) clearly shows the low-level character of the wave-like disturbance.

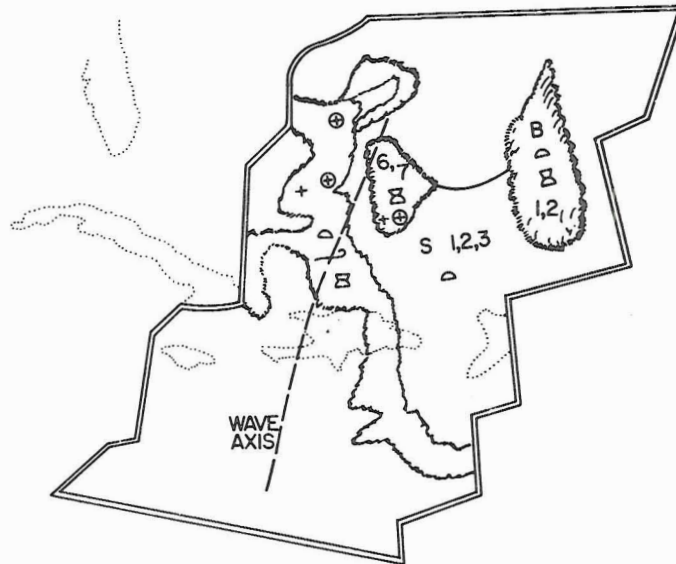
STRUCTURE OF THE WAVE

Examination of the streamlines at the various levels shows that the wave was most intense at 925 mb and decreased to nearly zonal flow at 600 mb. The axis of the wave was nearly vertical to 925 mb and then tilted with height; at 700 mb the axis was 150 miles east of the surface position. Figure 5 shows the streamlines and isotachs at the 850 mb level. While the isotach patterns were rather complex at each level, the general features of a maximum north of the center and a minimum to the south were present throughout.

The field of winds relative to the axis was obtained by subtracting the motion vector (285° at 16 knots) of the system from the actual winds read at the grid points shown in Figure 6. Figure 7 shows the relative streamlines and isotachs at the 850 mb level. Since steady state has been assumed, these streamlines are trajectories with respect to the wave. Since over a large part of the area the basic current speed u was nearly equal to the wave speed c , i.e. $u \approx c$, trajectories with large north-south amplitude with respect to the axis resulted. A closed relative wind circulation was present to the 700 mb level, but at 600 mb the air motion with respect to the axis was mainly from west to east with some north-south components in the central region. Again the isotach patterns were complex, but the maximum relative wind velocities were generally west of the wave with zero relative motion at a point near the axis.



(a) September 12, 1963 (1609 GMT)



(b) September 14, 1963 (1701 GMT)

Figure 3. Tiros VI pictures showing the distribution of clouds.

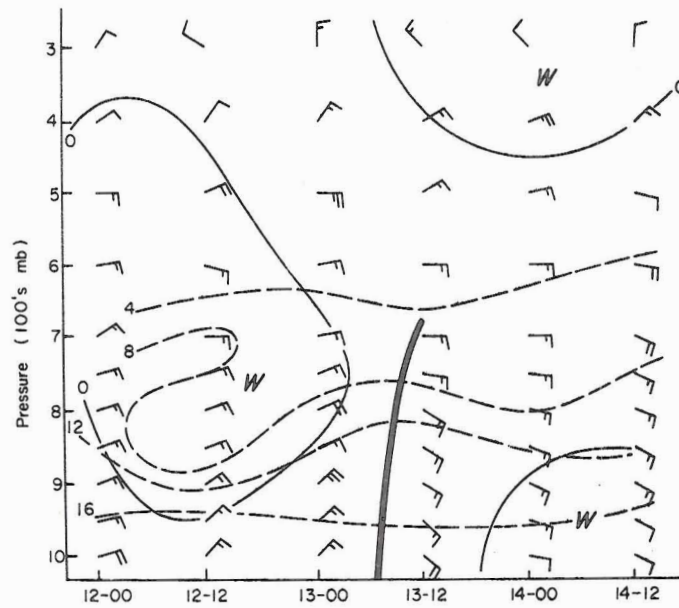


Figure 4. Time section for St. Maarten showing passage of the wave. Dashed lines show specific humidity distribution, while solid lines show temperature deviations from the mean across section. Long wind barb = 10 knots (— - 15 knots)

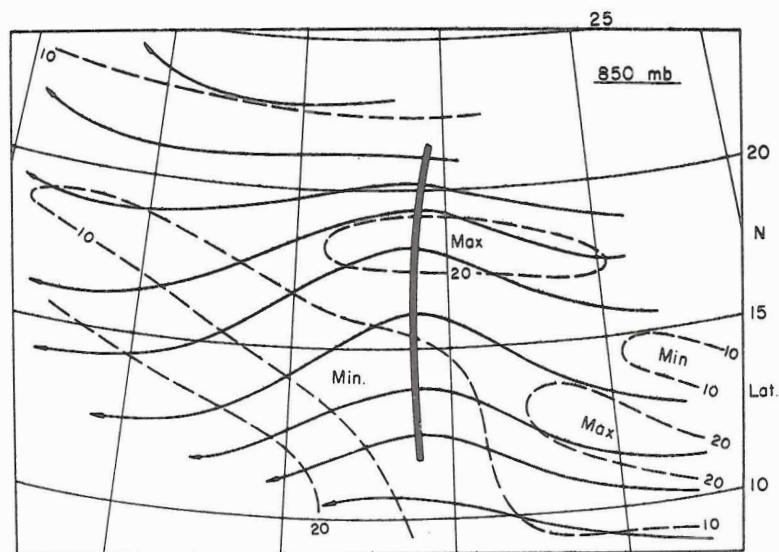


Figure 5. Streamlines (solid lines) and isotachs (dashed lines) at the 850 mb level from the composited wind reports. As in Figure 2 the latitude and longitude lines are for orientation.

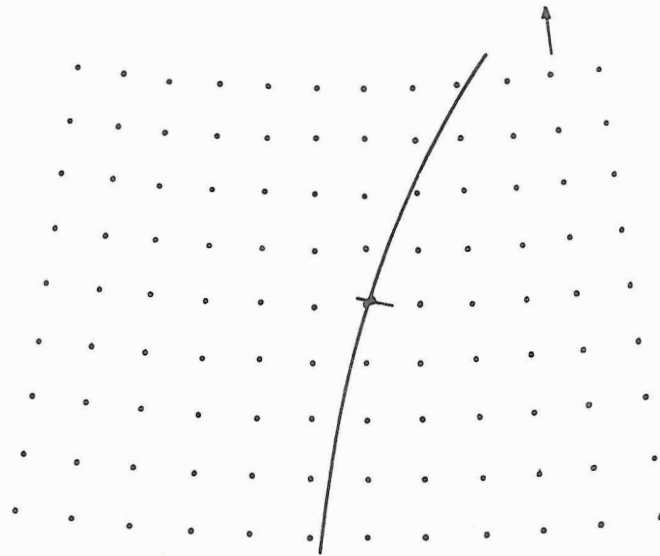


Figure 6. Grid on which computations were made. Spacing of the gridpoints is $1\frac{1}{2}^{\circ}$ latitude. Arrow at upper right is used for alignment.

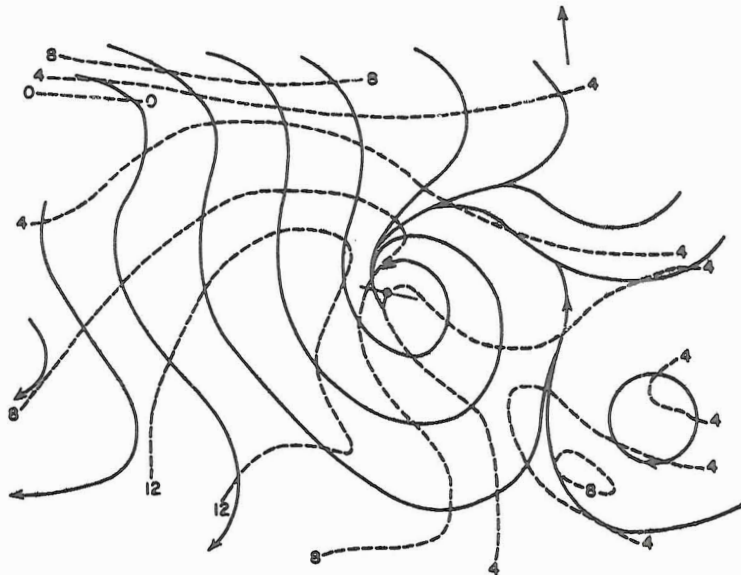


Figure 7. Relative streamlines and isotachs (knots) at the 850 mb level.

From the wind field, the absolute vorticity

$$\zeta = \frac{\partial v}{\partial x} + \frac{\partial e}{\partial y} + f$$

where v and $e = -u$ are the south and east wind speeds, and f is the Coriolis parameter, was computed at the gridpoints of Figure 6. At the lower levels the vorticity maximum was on the axis (see Figure 8 for 850 mb vorticity pattern). At the upper levels this maximum was displaced south and east, with a vorticity minimum in the northern region. These patterns bring out the cyclonic circulation present near the axis in the lower layers.

Whereas the composite wind field was easily analyzed, the thermal and moisture fields were more irregular. Diurnal effects as well as island effects were large, particularly in the lowest levels. Consequently smoothed temperature and moisture fields were derived by arithmetically averaging all the values in overlapping squares with sides of 3° latitude (or 180 n.m.). Then vertical profiles of the temperature and moisture were constructed at each point of the grid so that vertical consistency was assured.

Up to 775 mb the broad features of the temperature pattern (Figure 9) consisted of two relatively cold areas--one just to the east of the axis, the other well to the west of the axis--with a warm tongue extending over most of the southwest quadrant. This pattern was just opposite that noted by Yanai (1961) for a cold-core easterly wave in the Pacific Ocean. At 700 mb the temperature gradients were very small west of the axis. A relatively warm region was situated immediately east of the axis, with colder air still farther east. Thus throughout the layer up to 600 mb a relatively warm central core of air thought to be necessary for hurricane development was present.

In the lower layers the moisture field (Figure 10) had a broad maximum west of and close to the axis with a pronounced minimum to the east of the axis. Separate minima were also present to the west and the northwest at the 850 mb level. In the 600-700 mb layer the maximum was located west of the wave axis and the minimum to the east. The locations of the moisture maxima are in fair agreement with the shifting of the maximum in the vertical velocity field.

For the computation of the pressure-height fields and the kinetic energy balance, fields of virtual temperature were derived from the

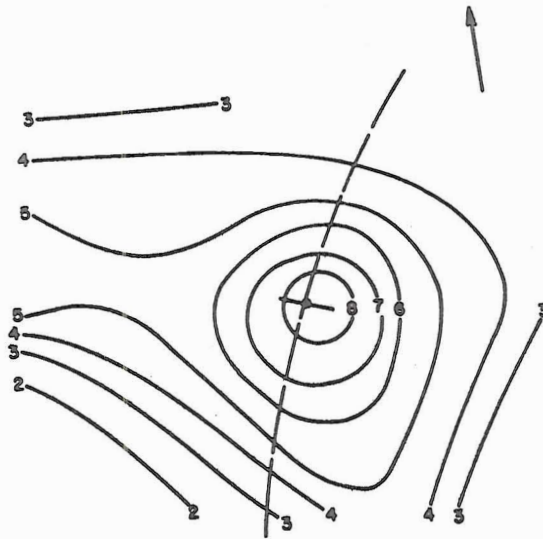


Figure 8. Absolute vorticity (10^{-5} sec^{-1}) at 850 mb.

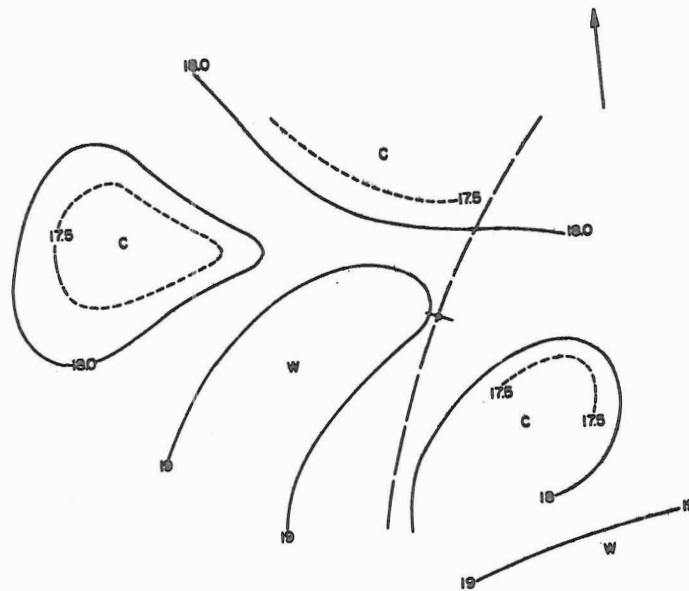


Figure 9. Dry-bulb temperature ($^{\circ}\text{C}$) at 850 mb from the soundings.

smoothed temperature and moisture fields. Since the moist and warm areas nearly coincide, the effect was to increase slightly the virtual temperature gradients over those of the dry temperature.

Equivalent potential temperature (θ_E) distributions were computed from the smoothed temperature and moisture profiles and compared with the composited distributions of θ_E from the soundings. While the "smoothed" 850 mb θ_E field was rather flat with a maximum range of 10 degrees, the nonsmoothed field showed more small-scale features with stronger gradients. At both lower and higher levels the gradients were weak. In general the patterns follow the moisture distributions closely.

MEAN VERTICAL MOTION

The potential vorticity theorem, $\frac{\zeta}{\zeta_0} = \frac{\Delta p}{\Delta p_0}$ which (1)

relates the changes in thickness Δp of a column with initial thickness Δp_0 (here taken as 75 mb) to the changes of absolute vorticity ζ along the trajectory, was used to compute the mean vertical motion fields. The vertical wind shear acting on the column of thickness Δp was used to adjust for some of the distortion of the column as it moved along the trajectory. In general the effect was to deflect the column trajectories toward the vorticity maximum in convergent regions, thus accenting the vertical motion. Likewise, in divergent regions the columns were deflected toward a lower vorticity region, which increased the rate of descent. The mean vorticity values ζ and ζ_0 were assumed to be the values at the midpoints of Δp and Δp_0 . The potential vorticity theorem could then be used to obtain the vertical displacement of the top of the column. Successive graphical additions for the various layers gave the field of vertical motion in terms of the substantial pressure derivative ω . Finally vertical profiles of ω were drawn for each gridpoint to assure vertical consistency.

Figures 11a and 11b show the field of mean vertical motion for the levels intermediate between 925 and 850 mb, and between 775 and 700 mb. At the lower levels the maximum ascending motion was north and just to the rear of the axis. The level of maximum ascending motion was near 810 mb. In Figure 11b the maximum ascent regions were on and ahead of the axis. At the 600 mb level the region of ascent was shrinking but the maximum velocities in a small region were still of the same order of magnitude as in Figure 11b.

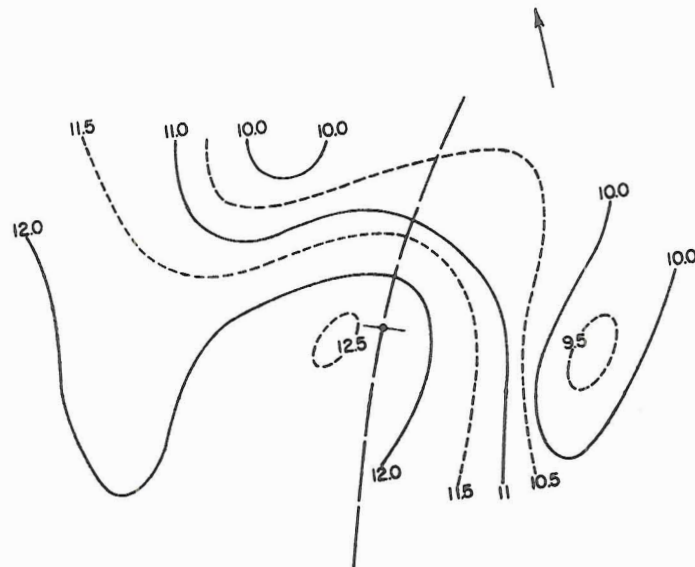


Figure 10. Specific humidity (gm/kg) at 250 mb level from the composited soundings.

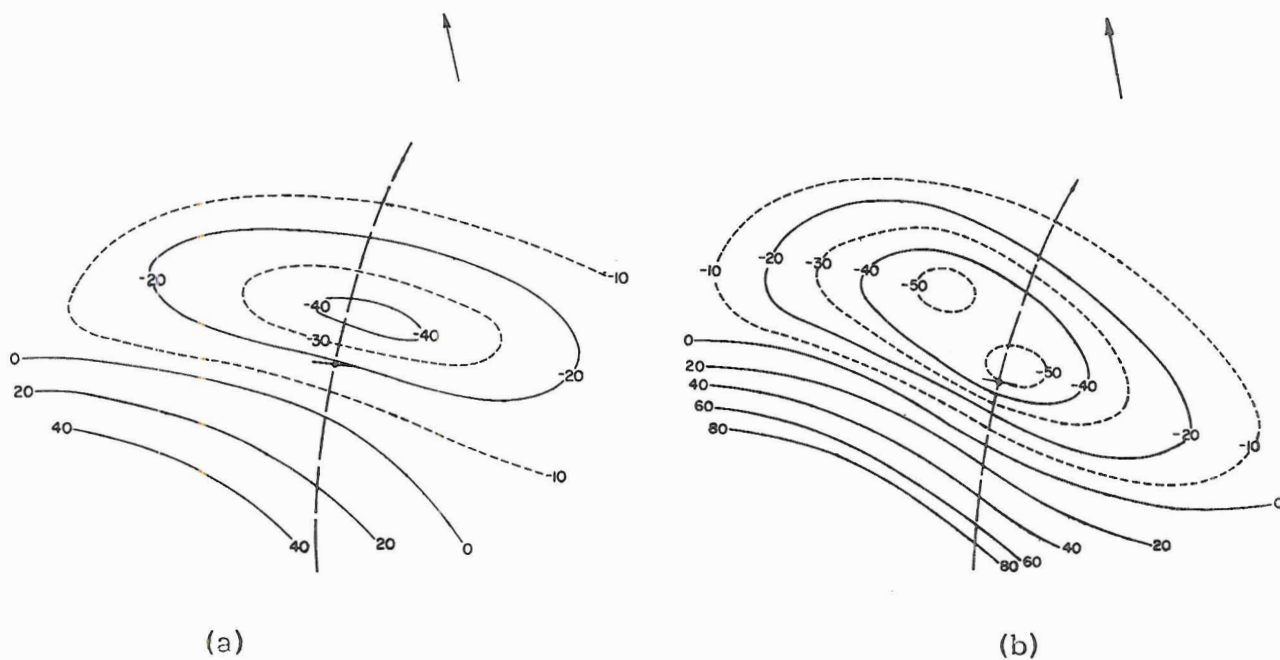


Figure 11. Mean vertical motion (mb/day) at (a) $387\frac{1}{2}$ mb (b) $737\frac{1}{2}$ mb derived from potential vorticity theorem.

TRAJECTORIES

In order to understand the thermodynamic processes which maintain the warm-core of the wave, an accurate description of temperature and moisture changes along particle trajectories is needed. Since the horizontal gradients of these quantities are not large, and the horizontal wind field is rather well-known, the problem is with changes due to vertical motions. Following a "mean" particle, i. e. using the mean vertical motion fields, assumes that the thermodynamics of the system are adequately described by rather slow adiabatic ascent in a non-diffusive atmosphere in which radiative cooling is the sink.

Use of the mean vertical velocity field for particle trajectories then provides the amount of radiative cooling required to offset the dry and/or moist adiabatic changes. Given a statistically adequate sample of trajectories at various levels, a comparison of the radiative cooling with the values known from previous climatological studies can be made. Agreement of the two values would indicate that the computed vertical motions are adequate on the basis of the implied model.

The trajectories for which this technique was used were those leading into the center of the region. Reasonable radiative coolings of 0.5 to 1.0°C/day were required to balance the extraction of heat, as the motion through the system was rather slow. While this seems to confirm the model, only a few trajectories could be followed over a long enough period of time to achieve a good estimate of the cooling. Consequently a careful examination of other cases, and eventually, an experiment with research aircraft will be required to verify the model.

One alternative to the use of any vertical motion assumption is following trajectories of columns which preferably extend throughout the atmosphere. This technique is realistic when the shear with height is small so that the columns remain intact to a sufficient approximation. The changes of θ_E profiles along a column trajectory are then indications of the processes which occur throughout the column, and the rate at which they occur.

Profiles of θ_E representative of the air moving from east to west through the wave were obtained from the soundings of 5 stations which throughout remained north of the center. In this case the averaged profiles were extended to 600 mb (Figure 12). These profiles can be interpreted as due to lifting of the entire layer. This is in contrast to the θ_E transformations in the cold core easterly wave which suggest a vertical

mixing of air brought about by evaporating rain (Riehl, 1965; Connell, 1965).

Using the relative streamlines, which did not vary much with height in the lower layers, a section along one of the incoming west-to-east trajectories was constructed. The θ_E profiles to 700 mb along this trajectory from 15 hours upstream to 15 hours downstream of the axis show the same form as those in Figure 12 but with less vertical displacement. It appears that, as the air moves along the trajectories, lifting of the entire layer is required, with the amount being comparable to the mean vertical motion. But as the difference between the two profiles is a net effect, it might also have been brought about by a large number of cumulus clouds vigorously mixing with their environment and thus not attaining great heights. That these clouds did not possess large downdrafts is evident since the θ_E profiles have nearly equal values near the surface. While the computations in this case appear to support the mean vertical velocity explanation, better temperature data than that afforded by compositing are required for a final conclusion.

MASS BALANCE

To compute the balance of energy which maintains the steady state wave, we need the mean mass circulation with respect to the wave. From the vertical motion fields the mean vertical mass flow through each pressure surface can be computed. The horizontal flow required for mass continuity was converted to a mean normal velocity \bar{c}_n and compared with the independent \bar{c}_n values obtained by averaging the values read at 12 gridpoints on the cylinder (Figure 13b). The \bar{c}_n values obtained from the vertical velocity field were approximately one third of the kinematic values. As the kinematic method is susceptible to small errors in the wind field, more confidence was placed in the \bar{c}_n profile from the vertical motion calculation. The mass balance for a 400 km radius cylinder is shown in Figure 13a. Since the smaller \bar{c}_n profile was used in the following energy budgets, the transport terms may be conservative.

KINETIC ENERGY BUDGET

Calculations of the energy budgets were made for the same 400 km radius cylinder with the axis at the center of circulation. For the kinetic budget the top of the cylinder was taken as the 600 mb surface. Then the balance of horizontal kinetic energy per unit mass $K = \frac{1}{2}v^2$ integrated over the mass inside the cylinder may be expressed as

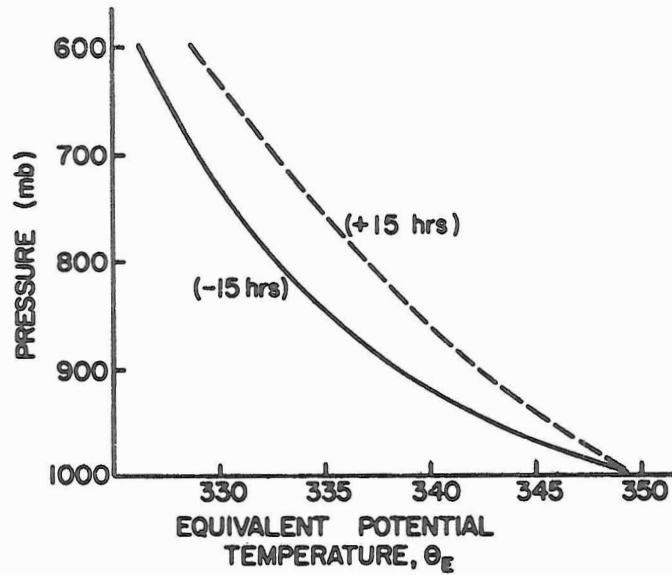


Figure 12. θ_E changes in columns 15 hours previous to and subsequent to wave passage just to north of center. Profiles are the average of the soundings at 5 nearby stations.

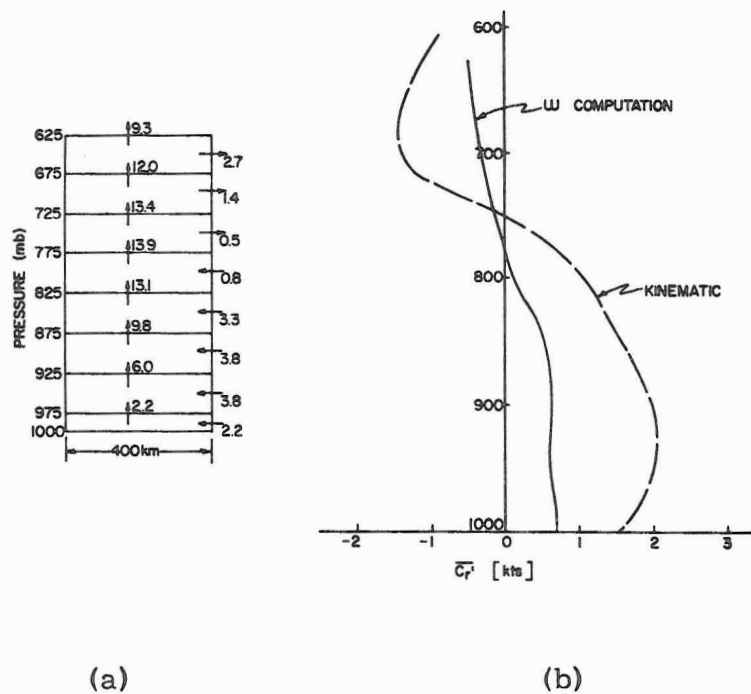


Figure 13. (a) Mass balance (10^{11} gm/sec) from the mean vertical motion fields. (b) Comparison of the \bar{C}_n (knots) profiles at 400 km obtained from the mass balance with those from kinematic computation.

$$0 = - \int_p \int_s K c_n \delta s \frac{\delta p}{g} - \int_p \int_s h c_n \delta s \delta p - R^* \int_p \int_A T_v \omega \delta A \frac{\delta \ln p}{g} +$$

$$+ \int_p \int_A \mathbf{v} \cdot \mathbf{F} \delta A \frac{\delta p}{g} \quad (2)$$

where the local change of the kinetic energy of the mass inside the cylinder $\frac{\delta K}{\delta t}$ has been equated to zero for the steady state system. In the above equation c_n is the normal velocity, h the geopotential height, R^* the gas constant, T_v the virtual temperature, ω the vertical velocity in pressure coordinates, \mathbf{v} and v the vector and scalar velocities, \mathbf{F} the frictional force per unit mass, and A the area of the pressure surface. The first term on the right represents the change in the kinetic energy due to the advection of kinetic energy by the mean flow through the surface of the cylinder. Since the vertical motion did not go to the zero at 600 mb there was also a small vertical advection of kinetic energy out of the cylinder. The second term in the equation represents the work done by pressure forces on the cylinder surface. This term contributes to an increase of kinetic energy in the lower layers which offsets a region near the 775 mb level where the system does work on the environment. Thus the first two terms tend to increase the kinetic energy of the mass within the cylinder, but, as we shall see, their contribution is small compared to that of the remaining two terms.

The importance of the warm-core nature of the wave is evident in the third term which represents the production of kinetic energy. Since the ascent for the most part takes place in warm regions, with descent in cooler regions, the associated release of potential energy tends to increase the kinetic energy of the system. Figure 14 shows a negative correlation of the deviations of the virtual temperature T_v and vertical motion ω from their area averages. The largest contribution to the negative correlation came from the layer 700-900 mb where the vertical motions and the virtual temperature gradients were largest. The negative correlation at the 625 mb surface appears to be due to the simultaneous shifts of the vertical motion and virtual temperature maxima to the same region ahead of the wave axis.

The kinetic energy balance is given in Table 1 where the residual (23.6×10^8 Kj/sec) represents the total frictional dissipation. The dissipation at the lower boundary may be estimated independently from

$-C_D \rho_0 V_0^3 A$ where C_D is a drag coefficient, ρ_0 the density at the surface of area A , and V_0 the velocity at the surface. Using $C_D \rho_0 = 1.8 \times 10^{-6}$ and the 1000 mb winds read at the gridpoints of Figure 6 for V_0 , the dissipation at the surface was $5.6 (10^8)$ Kj/sec. Therefore an internal dissipation of $18 (10^8)$ Kj/sec would be

TABLE 1

Summary of the Kinetic Energy Balance

Horizontal advection of kinetic energy into cylinder	$0.6 (10^8)$ Kj/sec
Vertical advection of kinetic energy into cylinder	$-0.2 (10^8)$
Pressure work on the boundary	$1.5 (10^8)$
Production of kinetic energy from release of potential energy	$21.7 (10^8)$
Balance - Total frictional dissipation	$-23.6 (10^8)$

required to make up the total in Table 1, but this value is unlikely. On the other hand, if the internal dissipation would have been assumed equal to the surface dissipation, the sum of the two (11.2×10^8 Kj/sec) would have represented the total frictional dissipation. The discrepancy between this sum and the 23.6×10^8 from the balance calculation is of the order of an acceleration of 10 kts/day of all the mass within the cylinder.

Since the system was observed to remain in nearly steady state, we could conclude from the horizontal kinetic energy balance that the warm core easterly wave generated kinetic energy which would appear to be balanced by an internal dissipation much above normally assumed values. While this is possible, we will later consider another explanation for this excess production of kinetic energy.

HEAT BALANCE

The balance of enthalpy $c_p T$ plus potential energy gz may be

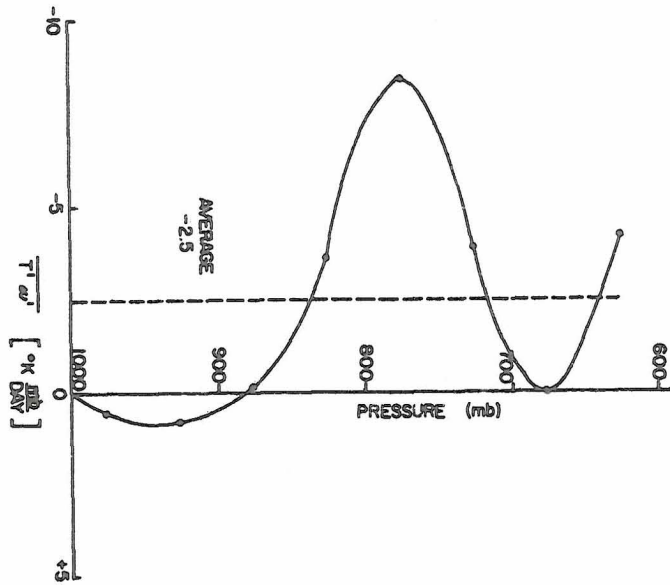


Figure 14. Vertical profile of the area averaged $T_v w$ correlation for the release of potential energy calculation.

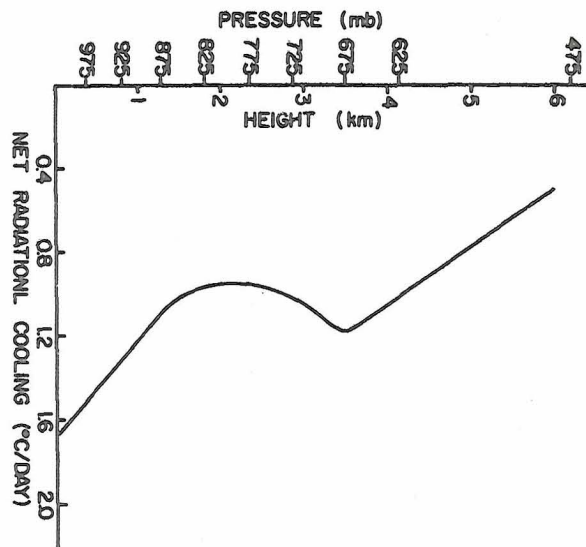


Figure 15. Net tropospheric radiation cooling ($^{\circ}C/day$) derived from Suomi-Kuhn radiometer data and London (1957) short wave radiation.

discussed separately from the balance of latent heat energy Lq , the two equations taking the following forms:

$$\iint (c_p T + gz) c_n \delta s \frac{\delta p}{g} + Q_s + LP - R = R^* \frac{\partial}{\partial t} \left[\iint T \cdot \delta A \frac{\delta p}{g} \right] + \frac{\partial}{\partial t} (E_e + E_p) = 0 \quad (3)$$

$$\iint L q c_n \delta s \frac{\delta p}{g} + Q_e - LP = \frac{\partial E_L}{\partial t} = 0 \quad (4)$$

where E_e , E_p , and E_L are the enthalpy, potential, and latent heat energy, with local changes with respect to time being set to zero in the steady state. In these equations Q_s and Q_e are the sensible and latent heat exchange between the air and ocean, R is the net tropospheric radiation, and P is the precipitation. As the above equations hold for any atmospheric layer, we will first discuss a balance for the entire region and then in the several layers making up the region.

Balance for Entire Region. In this case the quantities were integrated over a 400 km radius cylinder extending to the 475 mb surface where the mean vertical motion was assumed to vanish. The transport terms were evaluated from the \bar{c}_n profiles at the 400 km radius. Horizontal eddy transport of temperature and geopotential, but not of moisture, were neglected. The latter term contributes because of the increase in the depth of the moisture layer, so that the inflow is usually drier than the outflow. This was true at all levels in the present case and was a significant contribution to the latent heat balance.

As the surface wind speed and vertical specific humidity gradient were not exceptional in this case, the climatological value of evaporation was assumed (0.33 cm/day). In addition a Bowen ratio of 0.1 was assumed to determine the sensible heat transport at the sea surface. As will be seen later, the total heat balance in the subcloud layer gives a reasonable height of cloud base using these assumed sensible and latent heat exchanges with the ocean.

Riehl (1962) analyzed observations made over the Caribbean Sea with the Suomi-Kuhn infrared radiometer. Figure 2 of that paper gives the Oct. -Nov., 1960, long wave radiative flux which was also used in the present case. The profile for the short wave radiation was extracted from London (1957). The difference between the two curves

gives the net radiational cooling ($^{\circ}\text{C}/\text{day}$) profile used for this case (Figure 15).

Figure 16 shows the heat balance for the cylindrical region. In the latent heat balance on the left, the upper arrow represents the transport by the mean motion, the lower by the eddies. The eddy flow transports latent heat out of the region at all levels, while the mean flow transports moisture outward only above 775 mb. In the enthalpy plus potential energy budget the circled numbers represent the loss of heat from the region due to the radiational sink. Since the same amount of heat due to precipitation must enter as a heat loss to the moisture budget and a gain to the enthalpy plus potential energy budget, the amount of precipitation which occurred can be computed from each. In energy units, the precipitation amounted to $110 (10^{11})$ cal/sec in each budget, which was nearly equal to the evaporation of 3.3 mm/day when averaged over the area of 400 km radius. An independent check of this precipitation amount could not be made, but the amount is reasonable from the few observations available.

Heat Balance in the Layers. The above heat balance gives the transports of heat through the boundaries of the system; a more detailed balance within the layers of the system required a model specifying the vertical transport mechanism. As cloud physics has not developed sufficiently to provide the description of the convective currents forming the cumuli which effect the vertical heat exchange, a "statistical" cloud approach was used to describe the required exchanges between the cloud and the environment.

Ideally the cloud model would explain the features previously discussed: (1) An excess of horizontal kinetic energy over the dissipation was calculated on the synoptic scale. (2) From observations using the radar set at San Juan the cumulus clouds in the region (near the center) did not extend to great heights. Thus the cloud model should not possess large buoyancies which would shoot the clouds to great heights. Tiros VI and VII pictures show that the cloud coverage was not extensive. (3) The warm-core nature of the wave requires an explanation of the mechanism by which the heat is held in. (4) Large amounts of heat transferred from the ocean and imported by the low-level convergence must be redistributed vertically.

Cloud Model. The description of the heat exchange in the sub-cloud layer is not difficult if one neglects such effects as the evaporation of falling rain into the layer. A critical problem in this layer is the description of the roots of the cumuli by which the heat exchanges at upper levels are to take place. The mean sounding was not convectively

unstable in the subcloud layer unless rather high sea temperatures were assumed with a well-mixed subcloud layer. Thus the mean sounding was not representative of the air which actually formed the clouds. Rather these resulted from a selective process in which low level convergence cooperated with hot spots in the subcloud layer to provide the cumulus roots.

In the latent heat balance (4) for the subcloud layer (Figure 17) the vertical and horizontal transports of heat must balance the latent heat input Q_e from the ocean. A net convergence of 94 (10^{11}) cal/sec exists if the only mass transport through the cloud base is by the mean vertical motion. If this excess represents the vertical exchange accomplished by a saturated updraft of mass M' with specific humidity q_s through the cloud base, and a compensating downdraft in the clear air at specific humidity q_d of the mean sounding, the required eddy mass flow M' may be computed from

$$M' L (q_s - q_d) = 94 (10^{11}) \quad (5)$$

As an initial step we assume $T_s \approx T_d$ so that q_s is specified. With this value for the eddy mass transport the assumed equivalence of temperatures of ascending air and compensatory descending air can be verified with the enthalpy plus potential energy equation (3). Here again the precipitation $P = 0$ and the difference in geopotential heights of the ascending and descending currents assumed negligible. From equation (5), $M' = 38 (10^{11})$ gm/sec (or about 10 times the mean flow, see mass balance), and the required temperature difference $T_s - T_d$ at the 950 mb cloud base is 0.1°C , which verifies our previous assumption. Thus the convergence of warm air into the system by the mean motion and sensible heat transfer from the ocean to the atmosphere can be exported from the subcloud layer with this simple transport model.

In the upper layers it is tempting to propose a simple model which possesses entrainment and detrainment in equal amounts. Detrainment in this model includes those clouds which do not extend through the upper boundary, and entrainment includes those clouds which originate above the lower boundary. To test whether such a model is feasible, the latent and sensible heat equations can be written for a slab of cloud plus environment, requiring that the heat detrained from the cloud balance the radiation loss R in equation (3). All the liquid water that condenses is assumed to fall out so that no sensible heat is required to evaporate water detrained out of clouds. The properties at the middle of the layer are taken as being characteristic of the entraining and detraining air.

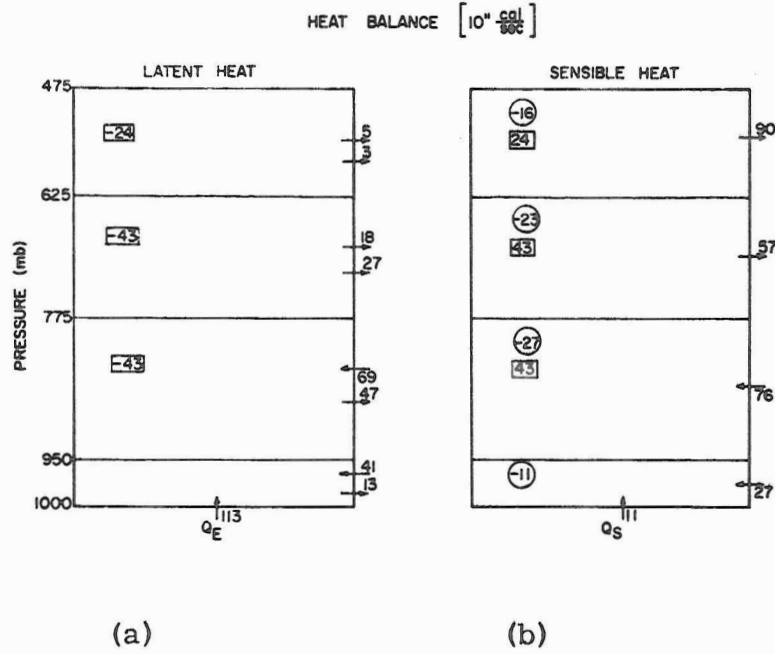


Figure 16. (a) Latent and (b) sensible heat balances (10^{11} cal/sec) for the 400 km cylindrical region. Lower latent heat transport arrow that by eddies. Circled numbers are the radiational cooling values. Numbers in small rectangles are the latent heat due to precipitation in each layer.

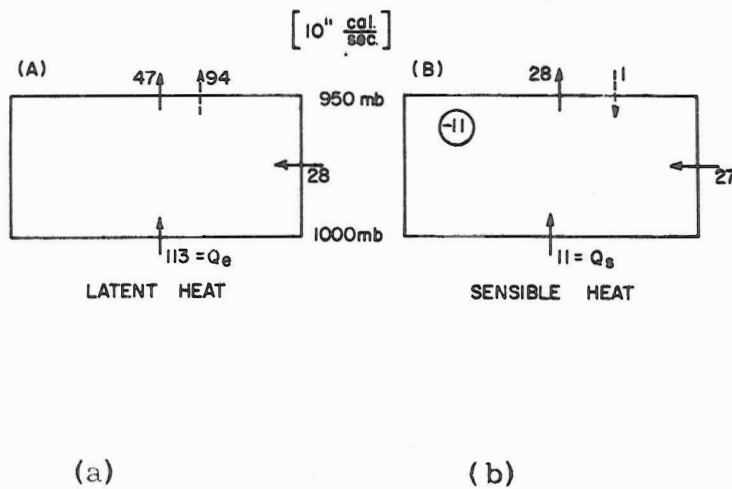


Figure 17. (a) Latent and (b) sensible heat balances (10^{11} cal/sec) for the subcloud layer.

The unknown in this case is the temperature of the detraining air which is assumed saturated. For the horizontal divergence of heat from the cloud to account for the radiation loss, the difference between the detraining and entraining air temperatures has to be large in order that the lateral mass flows not be very large. For the 925-775 mb layer this lateral mass flow was 44 (10^{11}) gm/sec or of the same magnitude as the vertical flow through the cloud base. Thus this simple entrainment model yields results of the correct order of magnitude, but is unacceptable as the model has no provision for limiting the vertical extent of the cloud.

As the first refinement the entrainment M_i and detrainment M_o were allowed to be different with compensating eddy mass flows M'_u (lower level) and M'_t (upper level) up in the clouds and down in the environment. Figure 18 shows the mass flow diagram which includes the lateral transport $M_1 = \overline{M}_u - \overline{M}_t$ through the 400 km radius cylinder. If the clouds occupy a very small fraction of the area, the radiational cooling may be assumed to occur only in the clear air. Then the balance of sensible heat $H = c_p T + gz$ for the entire layer may be written by multiplying each mass flow in Figure 18 by its corresponding sensible heat value H , with the d subscript denoting descending currents at mean sounding conditions. Sensible heat values at the bottom and top boundaries are represented by \underline{u} and \underline{t} subscripts respectively. Then with $Q_s = 0$ and steady state assumed, equation (3) for the layer may be written as

$$LP + \overline{M}_u H_u + M'_u (H_u - H_{ud}) = M_t H_t + M'_t (H_t - H_{td}) + M_1 H_1 + R \quad (6)$$

After eliminating M'_t by the continuity equation written with respect to the cloud

$$M'_t = M'_u + \overline{M}_u + M_i - \overline{M}_t - M_o \quad (7)$$

$$LP = - \overline{M}_u H_u + \overline{M}_u (H_t - H_{td}) - M'_u [(H_u - H_{ud}) - (H_t - H_{td})] + \overline{M}_t H_{td} + M_i (H_t - H_{td}) - M_o (H_t - H_{td}) + M_1 H_1 + R \quad (8)$$

The difference between sensible heat values inside and outside of clouds depends mainly on the temperature difference. Thus terms like $H_t - H_{td}$ are of the order of a few tenths of a calorie/gram, while the individual terms are of the order of 75 cal/gm (see Figure 19). Over pressure differences of greater than about 100 mb the vertical gradient of H becomes

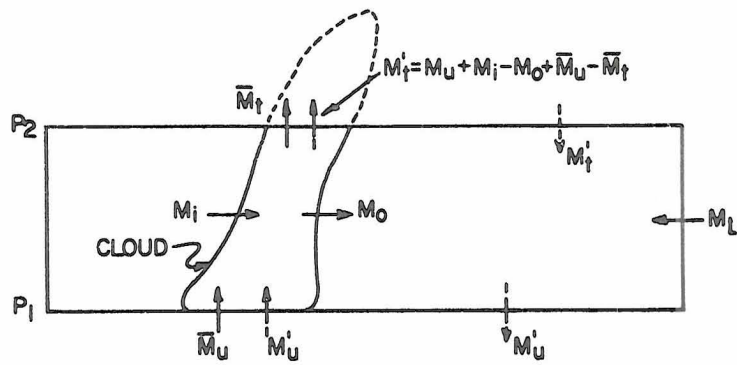


Figure 18. Mass flow diagram in statistical cloud for heat balance in layers.

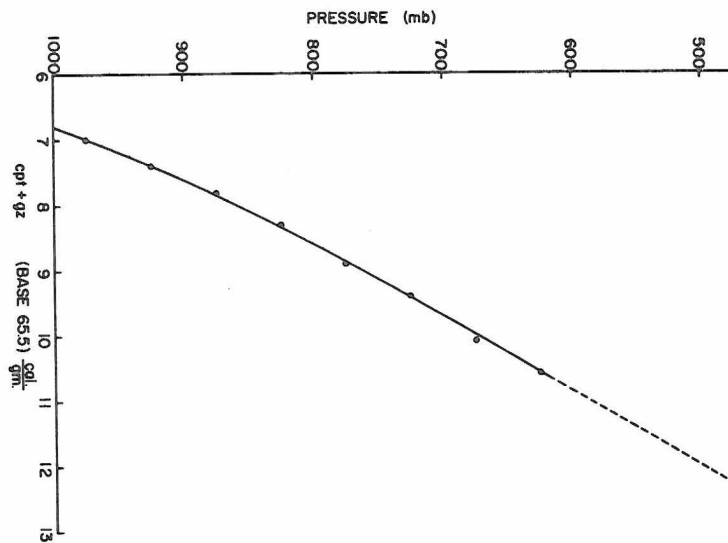


Figure 19. Sensible heat curve (base 65.5 cal/gm) for the mean sounding.

important, and only the first, second, fifth, eighth and ninth terms in equation (8) are important. When the appropriate values for the radiation and mean mass flows are inserted, the latent heat releases (10^{11} cal/sec) due to precipitation in each layer are: 950 - 775 mb, 43; 775 - 625 mb, 42; 625 - 475 mb, 24. The total, 109 (10^{11}) cal/sec, is within computational error of the latent heat release for the entire system.

We have thus determined the precipitation from equation (8) without the knowledge of the entrainment M_i and detraining M_o . These two unknowns, along with the total condensation C within the cloud, may be determined from the latent heat equation for the cloud plus environment, and the latent and sensible heat equations for the cloud alone. Again putting in the M'_t in terms of the remaining mass variables (see Figure 18), the latent heat equation (4) for the entire layer is completely analogous to (8)

$$\begin{aligned} -LP + \bar{M}_u L (q_u - (q_t - q_{t_d})) + M'_u L ((q_u - q_{u_d}) - (q_t - q_{t_d})) = \\ = \bar{M}_t L q_{t_d} + M_i L (q_t - q_{t_d}) - M_o L (q_t - q_{t_d}) + M_1 L q_1 \end{aligned} \quad (9)$$

Neglecting the radiational sink within the cloud, equations (3) and (4) written for the cloud depend on the divergence of heat plus the latent heat of condensation only. Again using the continuity equation (7) the latent and sensible heat balances for the cloud become

$$\begin{aligned} \bar{M}_u L (q_u - q_t) + M'_u L (q_u - q_t) + M_i L (q_i - q_t) - M_o L (q_o - q_t) - \\ - LC = 0 \end{aligned} \quad (10)$$

$$LC + \bar{M}_u (H_u - H_t) + M'_u (H_u - H_t) + M_i (H_i - H_t) - M_o (H_o - H_t) = 0 \quad (11)$$

where the subscripts i and o designate the values for the entraining and detraining air, respectively, and d the values in the descending current at either the bottom u or top t of the layer. In the above equations q_u , q_t , and q_o are taken as the saturation specific humidity values corresponding to the temperature of the mean sounding at that level, while q_i , q_{u_d} , and q_{t_d} are taken from the mean dew-point curve (Figure 20). The sensible heat values in the cloud and in the outflow were assumed to be 0.2 cal/gm larger than the values in Figure 19 which were taken for the remaining H values. This is equivalent to assuming that the ascending currents were 0.8°C warmer than the environment represented by the mean sounding. It is important

to note that in equations (10) and (11) the condensation C is used rather than the precipitation, since for the cloud balance it is the total heat of condensation released which is important. Finally the lateral latent heat transport term ($M_1 Lq_1$) was taken from the heat balance for the entire system (Figure 16) so that the transport by horizontal eddies was included.

Table 2 shows the summary of the solutions of equations (9), (10) and (11) for the three layers. Since the temperature and moisture values were not composited above 600 mb these values were extrapolated. The resulting values for the 625-475 mb layer were not consistent with the lower layers, but were included for completeness. The first column of the table shows the difference between the eddy vertical motion at the bottom M'_u and at the top M'_t of the layer. For the lower two layers there was less eddy ascent required at the upper level for heat balance, that is, the statistical cloud decreased in size with height.

Since the mean vertical motion was assumed to be zero at 475 mb, in the upper layer the heat balance must be accomplished by increased eddy mass transport through the upper boundary. The second column shows the part of this decrease/increase in eddy vertical motion due to an excess of detrainment over entrainment. In the third and fourth columns the actual values of the detrainment and entrainment are listed. In each layer these values were more than twice the eddy vertical motion through the bottom of the layer. The $M_i = 83.7 (10^{11})$ gm/sec for the 950-775 mb layer represents a mass flow rate such that all the air within that layer of the system would be brought into a cloud in 1-1/2 days. These large mass flow values were required for sensible heat balance because of the small difference between the sensible heat inside and outside of clouds. Some of this large value of M_i is due to the initiation of clouds above 950 mb, and is not entrainment in the normal sense. If representative, these entrainment-detrainment values represent the very active interaction between the clouds and their environment to accomplish the large scale heat balance. Or, looked at from a different point of view, there was an excess heat source when the system is treated by the statistical cloud approach.

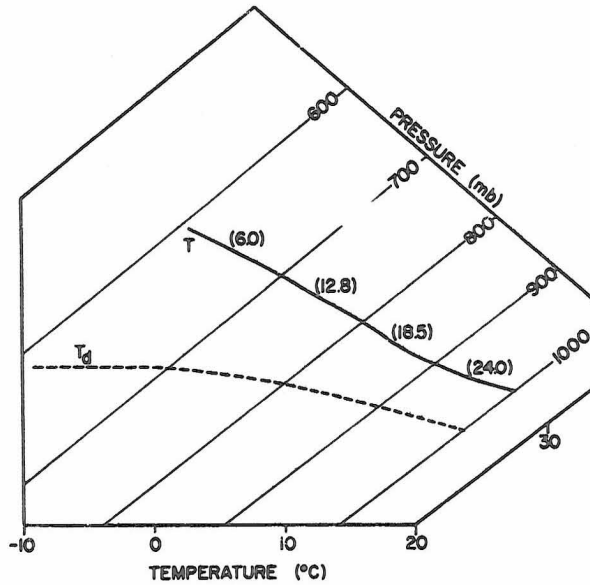


Figure 20. Tephigram showing mean dry- and wet-bulb soundings for the system. Numbers in parentheses are temperature values at 950, 850, 750 and 650 mb.

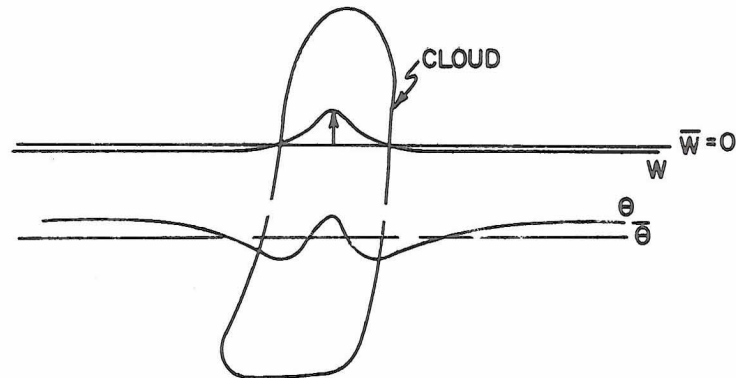


Figure 21. Proposed cloud model to increase the potential energy of the system. Mean profiles of vertical motion W and potential temperature θ through the clouds are shown.

TABLE 2

Summary of Heat Balance Calculations in Individual Layers

Layer	$M'_u - M'_t$	$M_o - M_i$	M_o	M_i	LP	LC	LP/LC
	(10 ¹¹ gm/sec)				(10 ¹¹ cal/sec)		
950-775	22.2	12.4	96.1	83.7	43	79	54%
775-625	6.9	11.4	53.0	41.6	42	51	83%
625-475	-7.8	1.5	33.0	31.5	24	36	67%

In the sixth column the total latent heat released by condensation of water vapor is shown. The ratio of this value to that released by precipitation gives a type of efficiency of the condensation process. One interpretation of this ratio is that there was a large fraction of clouds which did not extend through the 775 mb layer and thus did not precipitate out a large fraction of their condensate. But those clouds which extended into the second layer were effective precipitators, or at least did not detrain large amounts of condensate. We have previously noted that an enhanced eddy transport was required at 475 mb to accomplish the heat balance. This eddy transport resulted in a larger fraction of the condensate being advected through the upper boundary, with a consequent decrease in efficiency in this layer.

Thus a cloud model with all ascent in cloud, entrainment at the properties of the mean environmental sounding, detrainment of saturated air corresponding to mean environmental sounding plus 0.8°C, and eddy mass flow ascending in cloud and descending in clear air at the mean sounding properties has many features required for heat balance. Because soundings were not composited above 600 mb the computations in the upper layer were quite speculative. The computation showed a large convergence of heat into this layer by the mean motion which may not be realistic.

Alternative Cloud Model Accounting for Kinetic Energy Balance.

The above method of treating the clouds does not give any information as to the location of the clouds with respect to the axis or as to whether they could explain the observed synoptic-scale temperature gradients. On the cloud scale the ascent (as cumulus clouds) must be the result of buoyancy

forces, and the release of potential energy on this scale is assured. As noted above, rather intense interaction between the cloud and its environment was required by the heat balance calculations. This turbulent exchange of mass acts to dissipate the vertical kinetic energy and, in part, helps to explain the unbalance in kinetic energy.

One model in which both the heat and kinetic energy balances can be satisfied requires a forced circulation in such a way as to support cold cores surrounding the regions of active cloud ascent. Figure 21 shows schematically the mesoscale distribution of parameters required. In terms of the potential temperature θ , the core surrounding the region of active ascent should have the lowest values, while the active ascent region must have a higher value to allow for buoyant ascent. In the outer regions the descent should be associated with relatively high values of θ . It should be remarked that the heat balance would have to be fulfilled by an entirely different mechanism than used in the entraining-detraining model.

Several of the Woods Hole Oceanographic Institution expeditions to the tropics have noted the existence of "cold clouds" (Wexler and Wexler, 1960). In the present model it is essential that the cold core, which in the mean is dense with respect to its surroundings, be in part pulled up by the adjacent actively-ascending region and in part forced up by external pressure forces. Figure 22 shows a model suggested by H. Riehl for increase of potential energy by mesoscale circulation causing convergence in the convective system. We may assume a simplified kinetic energy equation of the form $\rho \frac{dK}{dt} = \frac{-u\partial p}{\partial x}$. If, as is shown in Figure 22, a positive correlation of the zonal wind component u and the pressure gradient $\frac{\partial p}{\partial x}$ is provided by the mesoscale convergence, a conversion of eddy kinetic to eddy potential energy will result. By contrast, isolated cumulus clouds in the tropics are usually observed to possess cold downdrafts which, of course, tend to release rather than store potential energy. However, it might be supposed that in a disturbance with its associated convergence, clouds of the type discussed above might exist and play an important part in the energetics of the disturbance.

The data from two Woods Hole Oceanographic Institution expeditions were examined to determine whether such a cloud structure had been observed. Temperature and moisture data read at 15 second intervals outside and 3 seconds inside clouds near Barbados were kindly provided by J. Levine. Additional data was taken from an unpublished manuscript on the 1956 Woods Hole Oceanographic Institution Caribbean expedition (R. Wexler and Malkus, 1958). As some problems remain with the "wet-bulb

effect" upon leaving clouds, only the data on the approach to the clouds were used. In particular the traces were examined to see if a decrease (noted in nearly every case) in dry-bulb temperature at the ascending outer edge of the cloud was associated with an increase in moisture. As the data were not taken specifically to study the air immediately outside of the cloud, the data interval of 15 seconds was rather large in that region. Numerous other problems, such as the method of determining exactly where the cloud began, have been discussed in the above report (R. Wexler and Malkus, 1958). It should also be noted that the age of the cloud is a rather important but unknown factor.

Keeping in mind the shortcomings in the data, we tried to determine whether the cloud model was worthy of further consideration and experimentation. Figure 23 shows the scatter diagrams of the decrease in dry-bulb temperature versus the increase in specific humidity. Qualitatively the expected correlation is present, but the scatter is large. As the cloud is approached (5 sec \approx 1/4 nautical mile) large differences in specific humidity increase occur for a given dry-bulb temperature decrease. The conclusion from these soundings was that the hypothesis was neither proved nor disproved, but that an experiment would have to be carried out to evaluate the hypothesis.

REMARKS

While one must be cautious in interpreting the results from composited data, it appears that the warm-core wave in the easterlies also is decisively influenced by the meso-structure (Riehl, 1965). The necessity for an intensive investigation with instrumented aircraft is evident to confirm a number of the features observed in the present case.

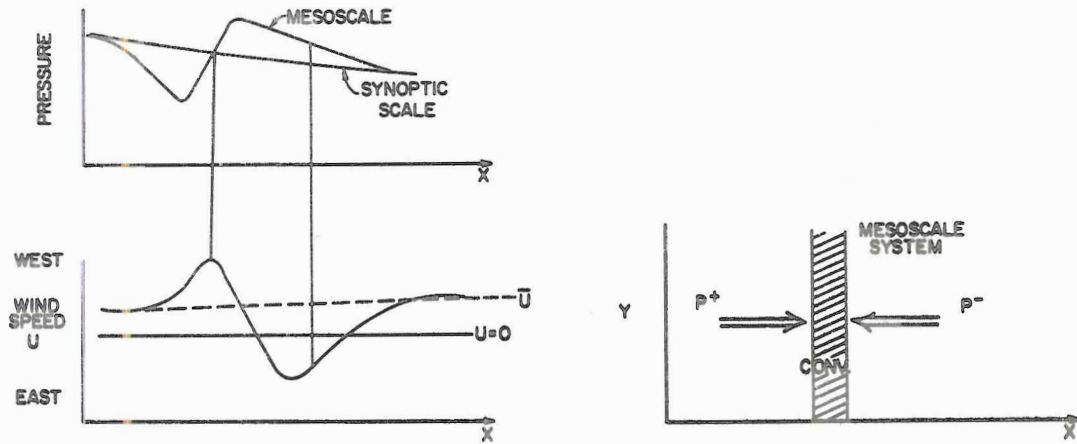


Figure 22. Model for increase of potential energy by meso-scale circulation in convective systems. (H. Riehl)

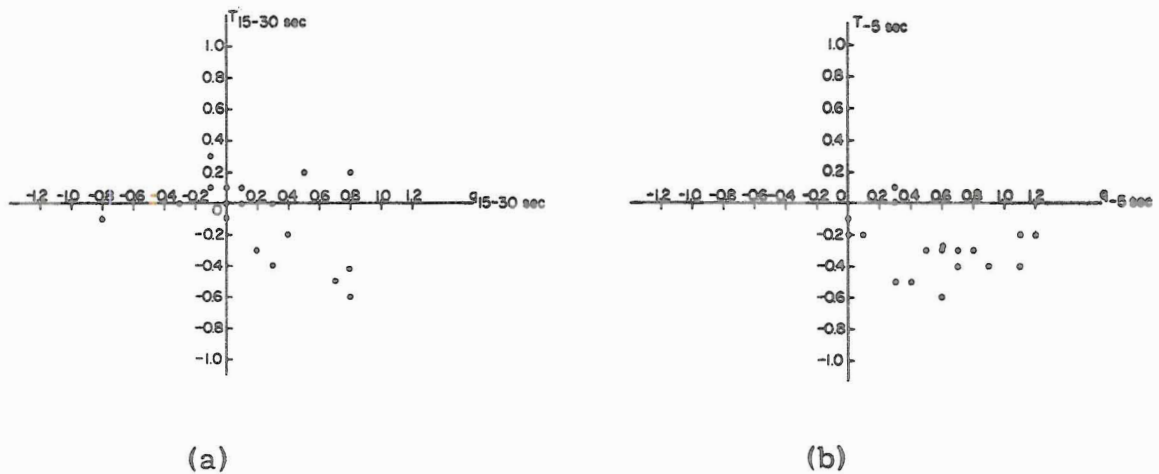


Figure 23. Scatter diagrams of the temperature and specific humidity changes on approaching clouds near Barbados. Incremental changes from (a) 30 to 15 sec and (b) 5 sec ($\approx \frac{1}{4}$ na. mi) to entry of cloud are correlated. (Data provided by J. Levine)

ACKNOWLEDGEMENTS

The author is indebted to Dr. Herbert Riehl, Department of Atmospheric Science, Colorado State University, who suggested this study and offered advice and encouragement throughout the investigation. Mr. William Plant assisted with some of the computations. Dr. Uwe Radok read the manuscript and offered many helpful suggestions. This research has been financially supported by the Environmental Science Services Administration. The author was supported by a National Aeronautics and Space Administration Traineeship during a portion of the study.

BIBLIOGRAPHY

- Connell, J., 1966: Unpublished M.S. Thesis, Colorado State University.
- Fett, R.W., 1965: The upper level structure of the formative tropical cyclone. Paper presented at 4th Technical Conference on Hurricanes and Tropical Meteorology, Miami, Florida.
- London, J.A., 1957: A study of the atmospheric heat balance. Dept. Meteor., New York University.
- Merritt, E.S., 1964: Easterly waves and perturbations, a reappraisal. J. Appl. Meteor., 3, 367-382.
- Riehl, H., 1945: Waves in the easterlies and the polar front in the tropics. Dept. Meteor., U. of Chicago, "Misc. Repts." No. 17.
- Riehl, H., 1959: On the production of kinetic energy from condensation heating. The Atmosphere and the Sea in Motion, ed. B. Bolin, Rockefeller Institute Press (New York), 381-399.
- Riehl, H., 1962: Radiation measurements over the Caribbean during the autumn of 1960. J. of Geoph. Res., 67, 3935-42.
- Riehl, H., 1965: Varying structure of waves in the easterlies. Paper presented at the International Symposium on Dynamics of Large Scale Processes in the Atmosphere, Moscow, USSR, June, 1965.
- Wexler, R., and Malkus, J., 1958: Observational studies of tropical clouds. Unpublished manuscript. Woods Hole Oceanographic Institution, Reference No. 58-46.
- Wexler, R., and Wexler, R., 1960: Cold clouds over tropical oceans. In Cumulus Dynamics, C.E. Anderson, ed., Pergamon Press (New York), 129-134.

Yanai, M., 1961a: A detailed analysis of typhoon formation.
J. of Meteor. Soc. of Japan, 39, 187-214.

Yanai, M., 1961b: Dynamical aspects of typhoon formation.
J. of Meteor. Soc. of Japan, 39, 282-309.